Korean J. Chem. Eng., **30**(3), 598-604 (2013)
DOI: 10.1007/s11814-012-0207-9

Low-temperature CO oxidation over water tolerant Pt catalyst supported on Al-modified CeO_2

Jung-Hyun Park*, Jun Hee Cho*, Sung Eun Kang*, Kyung Ho Cho, Tae Woo Lee***, Hyun Sik Han***, and Chae-Ho Shin*,†**

*Department of Chemical Engineering, Chungbuk National University, Cheongju, Chungbuk 361-763, Korea
**Green Chemistry Division, Korea Research Institute of Chemical Technology, Yuseong, Daejeon 305-600, Korea
***R&D Center, Heesung Catalysts Corp., #507-1Da, Jungwang-Dong, Shiheung-City, Gyeonggi-do 429-450, Korea
(*Received 25 September 2012 • accepted 23 November 2012*)

Abstract−A series of xAl-(1-x)Ce oxides (x=0-0.20) were prepared as supports by the coprecipitation method. 1 wt% Pt was impregnated on the Al-modified Ce oxide supports, which were tested as catalysts for CO oxidation in the absence and presence of H_2O vapor. The prepared catalysts were characterized by X-ray diffraction (XRD), N_2 sorption, CO temperature-programmed reduction (CO-TPR), ^{27}Al magic-angle spinning (MAS) NMR, and CO-chemisorption analyses. Upon comparison of the catalytic results obtained from the 1 wt% Pt/xAl-(1-x)Ce oxide catalysts, the Pt/0.10Al-0.90Ce oxide catalyst was found to exhibit the highest catalytic activity. When water vapor was present in the feed stream, the catalytic activity increased remarkably, and $T_{90\%}$ shifted to a temperature ca. 30 °C lower compared to that in dry conditions due to the promotion effect by the water-gas shift reaction. The catalytic activity could be correlated with the Pt dispersion and the amount of surface or lattice oxygen.

Key words: Platinum, Al Modified CeO_2, CO Oxidation, CO-TPR, ^{27}Al MAS NMR

INTRODUCTION

Although the oxidation of carbon monoxide is a simple reaction, it is very important for various applications in industrial process, transportation and domestic activities [1-3]. It is well known that noble-metal catalysts are favored choices for the oxidation of CO [4,5]. Platinum has been used widely as an active metal for catalysis in reactions such as hydrogenation, dehydrogenation and the catalytic removal of pollutants from automobile exhaust emissions [6]. In general, Pt is supported on various oxides such as alumina, silica, zirconia, and ceria [7-10].

A metal modified-support is used to obtain a high dispersion of metal catalyst or an improvement in the number of active sites for the catalytic reaction. Such surface modification significantly enhances the dispersion, the interaction between the metal particles and the support, and the thermal stability of platinum supported on silica, which are crucial factors affecting the catalytic activity [11].

Ceria, which has been investigated and applied widely for the oxidation reaction, has attracted much attention as either a catalyst or an oxygen storage/release component in ceria-based catalyst systems for the control of emissions from automobiles [12]. Al_2O_3, TiO_2, CeO_2, SiO_2 and mixed oxides with a high surface area and high mechanical stability are generally used as supports [13-15]. Well dispersed precious metal catalysts supported on ceria-modified Al_2O_3 are also used for the catalytic combustion of volatile organic compounds [15]. A 1 wt% loading of CeO_2 enhances Pt dispersion on an Al_2O_3 support and improves the stability of Pt against thermal sintering [16]. Thus, the nature of the support has a remarkable influence on the properties and activity of the catalysts.

We investigated the oxidation of CO on Pt supported on ceria and Al-modified Ce oxide with different Al loadings (xAl-(1-x)Ce, x=0-0.20). The catalysts were characterized using X-ray diffraction (XRD), N_2 sorption, CO temperature-programmed reduction (CO-TPR), CO temperature-programmed desorption (CO-TPD), ^{27}Al magic-angle spinning (MAS) NMR, and CO-chemisorption analysis to determine their physicochemical properties. The information derived from the results of these analyses was correlated with the CO oxidation activity. We focused on the correlation between the catalytic activity of CO oxidation and the amount of surface or lattice oxygen in the Pt/xAl-(1-x)Ce oxide catalysts with different Al contents.

EXPERIMENTAL

1. Catalyst Preparation

xAl-(1-x)Ce mixed oxides (molar ratio x=0-0.20) were prepared as supports using a coprecipitation method. Known amounts of $Ce(NO_3)_3 \cdot 6H_2O$ (Junsei, >99%) and $Al(NO_3)_3 \cdot 9H_2O$ (Junsei, >98%) were dissolved in de-ionized water. NH_4OH solution (SK Chemicals, 28 vol%) was added to the mixed salt solution under vigorous stirring and the solution pH was adjusted to 10. The resulting solution was aged at 70 °C for 24 h with vigorous stirring, then filtered, washed with de-ionized water, and dried at 100 °C for 12 h. The catalysts were then calcined in an air flow at 500 °C for 2 h.

The 1 wt% Pt/xAl-(1-x)Ce oxide catalysts were prepared by the incipient-wetness impregnation method using an aqueous solution of $Pt(NH_3)_4(NO_3)_2$ (Aldrich, 99%). The catalysts were dried at room temperature for 12 h and calcined at 500 °C for 2 h under flowing air.

†To whom correspondence should be addressed.
E-mail: chshin@chungbuk.ac.kr

2. Catalyst Characterization

The crystalline structures of the catalysts were analyzed with a Siemens D5005 diffractometer with CuK_α radiation operating at 30 kV and 50 mA at a scanning rate of 0.4° min^{-1}. Phases were identified by matching the experimental patterns to the JCPDS powder diffraction file (01-081-0792). The crystalline particle size was calculated by using the Scherrer's equation. The Brunauer-Emmett-Teller (BET) surface area was measured by N_2 sorption analysis using a Micromeritics ASAP 2020 instrument. Prior to measurement, each sample was degassed for 4 h under vacuum at 250 °C. Temperature-programmed reduction experiments employing CO (CO-TPR) were carried out by using a Pfeiffer OmniStar mass spectrometer (MS) as a detector. Before analysis, the sample (0.05 g) was loaded in a quartz reactor (I.D. 12 mm) and pretreated at 300 °C in a He flow (50 cm^3 min^{-1}) for 1 h. After cooling to RT, a flow of 5% CO/N_2 was introduced through the samples and the temperature was increased from RT to 900 °C at a rate of 10 °C·min^{-1}. The mass signals of m/z=2 (H_2), 28 (CO), 18 (H_2O), and 44 (CO_2) were detected by MS.

The ^{27}Al MAS NMR spectra were obtained on a Bruker AVANCE 500 spectrometer, at a ^{27}Al frequency of 130.325 MHz, in a 4 mm rotor at a spinning rate of 10.0 kHz. The spectra were obtained with an acquisition of approximately 3000 pulse transients, which were reported with a $\pi/4$ rad pulse length of 1.50 ms and a recycle delay of 1.0 s. The ^{27}Al chemical shifts are reported relative to $Al(H_2O)_6^{3+}$ solution.

The platinum dispersion was determined by static volumetric CO-chemisorption using a Micromeritics ASAP 2020C instrument. Prior to the adsorption experiments, the sample (0.5 g) was placed in a quartz cell, degassed at 100 °C for 1 h, then re-reduced in H_2 at 400 °C for 2 h and evacuated at the same temperature for 1.5 h. The sample was cooled under vacuum to the adsorption temperature, and the chemisorption measurements were performed at 35 °C. The chemisorption isotherm was obtained from the difference between the first adsorption isotherm, which is the sum of chemisorption and physisorption and the second adsorption isotherm, which is from the physisorption. The amount of chemisorbed CO on the platinum was obtained by plotting the amounts of adsorbed CO as a function of the partial pressure of CO and back extrapolating to zero. The metal dispersion was calculated assuming a CO/Pt stoichiometry of 1.0.

To prove the promoting effect of water vapor on CO oxidation, CO oxidation was carried out over the Pt/0.10Al-0.90Ce oxide catalyst at 70 °C under atmospheric pressure by using a fixed-bed quartz reactor. Before analysis, a 0.04 g sample was loaded in a quartz reactor (I.D. 12 mm) and pretreated at 400 °C in a H_2 flow (50 cm^3 min^{-1}) for 1 h and then cooled to 70 °C under an Ar flow (50 cm^3 min^{-1}). The gas mixtures consisted of 1% CO and 4% O_2 balanced in Ar, and the total flow rate was 100 cm^3 min^{-1}. Mass signals of m/z=2 (H_2), 28 (CO), and 44 (CO_2) were detected.

CO and CO_2-temperature programmed desorption (TPD) experiments were performed in the same quartz reactor. Before analysis, a 0.04 g sample was loaded in a quartz reactor and pretreated at 400 °C in a H_2 flow (50 cm^3 min^{-1}) for 1 h, and then cooled to 70 °C under an Ar flow (50 cm^3 nin^{-1}). After cooling to RT, the adsorbents (10% CO+5% O_2 in balanced in Ar (dry), and addition of 5% H_2O (wet) for CO-TPD, and pure CO_2 (30 cm^3 min^{-1}) for CO_2-TPD) were passed out on the catalyst bed at a flow rate of 50 cm^3 min^{-1} for 30 min. Then, the samples were heated to 600 °C at a heating rate of 10 °C min^{-1}. The mass signal of m/z=44 (CO_2) was detected by MS.

3. Catalytic Test for CO Oxidation

The catalytic oxidation of carbon monoxide was performed in a continuous-flow, fixed bed reaction system with a quartz reactor (I.D. 12 mm) at atmospheric pressure. Each catalyst (0.02 g) with SiC (1 g) as a diluent was loaded in the reactor and pretreated at 400 °C in the H_2 flow for 1 h, prior to the catalytic reaction. The dry feed stream was 1% CO, 4% O_2, and 95% He by volume, with a total flow rate of 200 cm^3 min^{-1}, and was heated at a rate of 2 °C min^{-1} from 40 to 160 °C. In addition, for the examination of the effect of water vapor, 3% H_2O vapor was introduced continuously into the reactor through the saturator. The conversion of carbon monoxide in the reaction was calculated in terms of the percentage consumed. The concentration of carbon monoxide in the product stream was measured every second by using an on-line CO analyzer (TELEDYNE Instrument Analyzer of IR-ways).

RESULTS AND DISCUSSION

1. Characterization

The XRD patterns and crystallite size of the Pt/xAl-(1-x)Ce oxide catalysts with different Al molar ratios are shown in Fig. 1 and Table

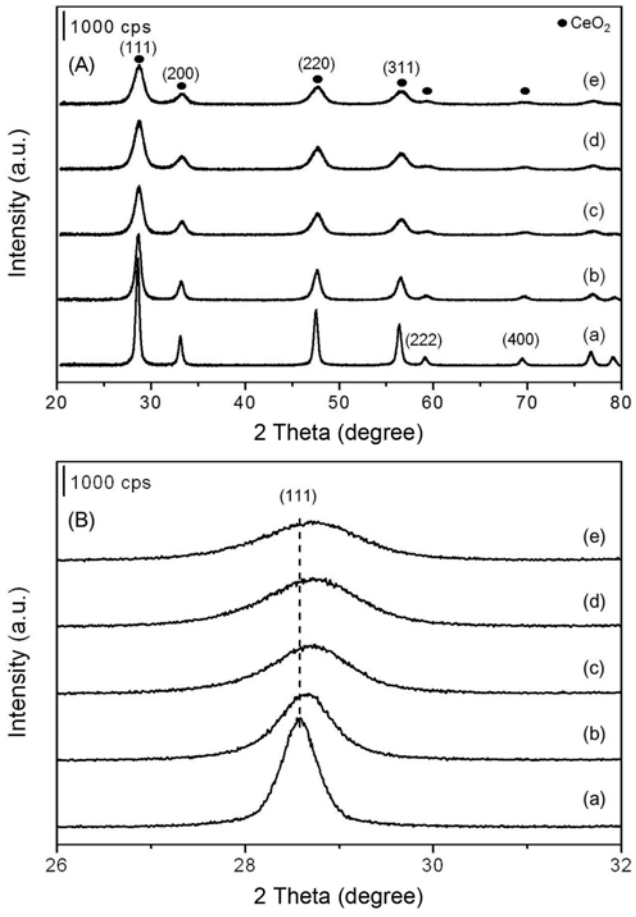

Fig. 1. XRD patterns (A) of Pt/xAl-(1-x)Ce oxide catalysts and (B) more detailed diffractograms in the region 2θ=26°-32°: (a) Pt/CeO_2, (b) x=0.05, (c) 0.10, (d) 0.15, and (e) 0.20.

Table 1. Physico-chemical properties of 1 wt% Pt/xAl-(1-x)Ce oxide catalysts and their catalytic activities for CO oxidation

x in Pt/xAl-(1-x)Ce	Crystallite size (nm)[a]	Lattice constant (nm)[b]	S_{BET} ($m^2 \cdot g^{-1}$)	Pore volume ($cm^3\ g^{-1}$)	Dispersion (%)[c]	Relative amount of CO_2[d]	Dry conditions[e]		Wet conditions[f]	
							$T_{50\%}$	$T_{90\%}$[g]	$T_{50\%}$	$T_{90\%}$
CeO_2	26.3	0.5412	50	0.222	59	2.164	115	127	79	87
0.05	14.5	0.5402	74	0.212	82	2.191	105	118	74	79
0.10	9.6	0.5396	103	0.278	84	2.319	103	114	71	75
0.15	9.4	0.5393	122	0.253	69	2.076	114	126	72	85
0.20	8.6	0.5387	126	0.293	56	1.892	119	130	85	92

[a]Calculated from line broadening of the CeO_2 (111) peak using the Scherrer equation
[b]Lattice constant of pure CeO_2=0.5412 nm
[c]Calculated by CO chemisorption analysis
[d]Calculated from CO-TPR analysis
[e]$CO/O_2/N_2$=1/4/95, F/W=26.8 mol h^{-1} g_{cat}^{-1}
[f]3% H_2O vapor was supplied continuously
[g]Temperature in Celsius at which 50 and 90% conversion were reached, respectively

1. The major intensity peaks of the CeO_2 phase are detectable for all of the samples. However, the crystalline phases of the Pt species and Al_2O_3 were not observed, indicating that the Pt species was highly dispersed or its particle size was so small that the signals could not be detected by XRD analysis. With increasing the Al molar ratio, the relative intensity of the CeO_2 peaks decreased, and the peaks of the Pt/0.20Al-0.80Ce oxide catalyst were broader than those of the other catalysts, indicating that the Pt/0.20Al-0.80Ce oxide catalyst had the smallest crystallite size. The crystallite sizes of the CeO_2 in the Pt/xAl-(1-x)Ce oxide catalysts decreased from 26.3 to 8.6 nm with increasing Al molar ratio. The lattice constant of the ceria in the Pt/CeO_2 catalyst was 0.5412 nm [17]. The addition of Al retracts the lattice of cubic CeO_2; thus, the lattice constant decreased from 0.5412 nm in pure CeO_2 to 0.5387 nm in the 0.20Al-0.80Ce oxide support (Fig. 1(B) and Table 1). This result indicates that the lattice of the CeO_2 shrinks owing to the insertion of Al^{3+} into CeO_2 lattice. Since the radius of the Al^{3+} cation (0.068 nm) is smaller than that of the Ce^{3+} (0.115 nm) and Ce^{4+} cations (0.101 nm), the Al^{3+} cation can be inserted into the CeO_2 lattice [18]. Thus, the insertion of the Al cation into the ceria lattice could lead to the formation of pure xAl-(1-x)Ce with x in the range 0.0-0.2.

Table 1 lists the surface areas and total pore volumes of the 1 wt% Pt/xAl-(1-x)Ce oxide catalysts. The N_2 sorption isotherms of all the catalysts are of type IV, which is typical of mesoporous samples (Fig. 2). The catalysts exhibit a significant increase in the S_{BET} value with increasing Al molar ratio. From Table 1, it can be seen that upon increasing the Al molar ratio from 0.05 to 0.25, the BET surface area of the catalyst increases from 74 to 126 $m^2\ g^{-1}$, and the pore volume also increases from 0.212 to 0.293 $cm^3\ g^{-1}$. This phenomenon can be attributed to the fact that the Al-modified CeO_2 support obtained by the insertion of Al^{3+} cations into the CeO_2 lattice is more stable than pure CeO_2 after calcination at 500 °C.

Although the H_2 chemisorption method is widely applied to determine the dispersion of active metals due to no dependence of the stoichiometry on the metal sizes, the dispersion of Pt on Al modified Ce oxide catalyst determined by H_2 chemisorption was not easily controllable due to the hydrogen spillover phenomenon. Thus, the CO chemisorption method was used to determine the dispersion of Pt metal.

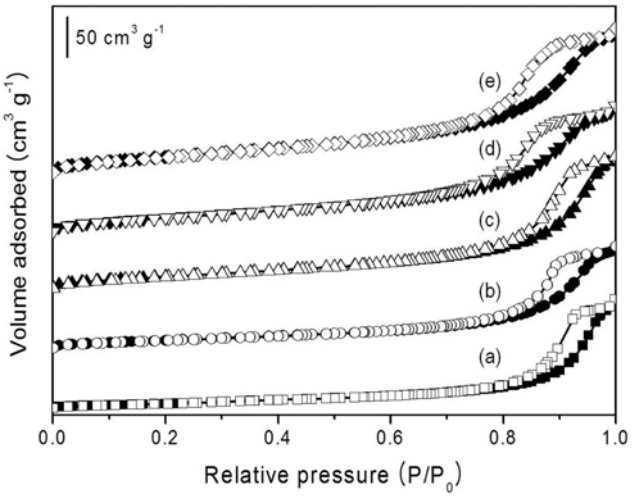

Fig. 2. N_2 adsorption-desorption isotherms of Pt/xAl-(1-x)Ce oxide catalysts: (a) Pt/CeO_2, (b) x=0.05, (c) 0.10, (d) 0.15, and (e) 0.20.

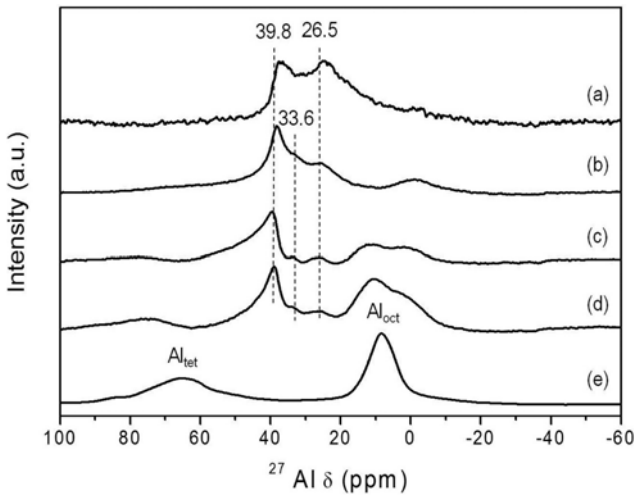

Fig. 3. ^{27}Al MAS NMR spectra of xAl-(1-x)Ce oxide supports: (a) x=0.05, (b) 0.10, (c) 0.15, (d) 0.20, and (e) Al_2O_3.

CO chemisorption experiments were performed for the measurement of the Pt dispersion in Pt/xAl-(1-x)Ce oxide catalysts as shown in Table 1. The Pt/0.10Al-0.90Ce oxide catalyst shows the highest dispersion among the catalysts investigated here. The dispersion decreased in the order Pt/0.10Al-0.90Ce>Pt/0.05Al-0.95Ce>Pt/0.15Al-0.85Ce>Pt/CeO_2>Pt/0.20Al-0.80Ce.

Fig. 3 shows the ^{27}Al MAS NMR spectra of the Al-modified CeO_2 oxides and of pure γ-Al_2O_3 for comparison. The NMR spectrum of γ-Al_2O_3 (Fig. 3(e)) shows two peaks at 64.9 and 8.2 ppm, which are assigned to tetrahedrally and octahedrally coordinated Al^{3+}, respectively [19,20]. In the results for the xAl-(1-x)Ce oxides, new peaks appear at 27, 34, and 40 ppm. The peak at 26.5 ppm gradually decreases as the Al content increases. With increasing CeO_2 concentration, the relative intensities of Al_{oct} and Al_{tet} decrease, and these peaks disappear completely for the 0.05Al-0.95Ce oxide support. This indicates that a different species containing Al^{3+} is present in the xAl-(1-x)Ce mixed oxides. The NMR spectrum of the 0.10Al-0.90Ce, 0.15Al-0.85Ce and 0.20Al-0.80Ce oxides shows a peak at 34 ppm, which is assigned to pentacoordinated Al^{3+}, and a shoulder peak at around 0 ppm is observed with increasing Al molar ratio, which is assigned to octahedrally coordinated Al^{3+} from $CeAlO_3$ [21]. The peak observed at 26.5 ppm is attributed to Al^{3+} that has interacted with Ce^{3+} [22]. The peak at around 40 ppm is attributed to the limited solubility of Al^{3+} ions in the CeO_2 lattice. Since the radius of the Al^{3+} cation is smaller than those of the Ce^{3+} and Ce^{4+} cations, the Al^{3+} cations can diffuse into the CeO_2 lattice, while the diffusion of Ce^{3+} or Ce^{4+} cations in the Al phase is expected to be difficult [18]. The formation of a bulk solid solution between the aluminum and cerium species is hindered owing to the difference in ionic radius between the Ce^{4+} and Al^{3+} ions. Therefore, this peak is assigned to the Al^{3+} ions, which can be dissolved in the CeO_2 lattice.

2. CO-TPR

The CO-TPR profiles for the Pt/xAl-(1-x)Ce oxide catalysts are shown in Fig. 4. Several kind of CO_2 peaks from the oxidation of CO adsorbed with oxygen species on the Pt/xAl-(1-x)Ce oxide catalysts are observed for all the catalysts (Fig. 4(A)). The first CO_2 peak in the range 50-200 °C (denoted as O_{s1}) is absent on the Pt-free Al-Ce mixed oxides and the CeO_2 (not shown). This peak is therefore from the reaction of CO with oxygen adsorbed on the metallic Pt particles [23]. The O_{s1} peak position, centered at approximately 100 °C, is almost the same for all the catalysts, indicating that all the catalysts have a similar PtO_x reducibility. CO_2 production in the medium-temperature range 200-550 °C (denoted as O_{s2}) was observed as the reaction between CO was adsorbed on the support and surface oxygen of the Al-Ce oxide. The surface oxygen species, O_{s1} and O_{s2}, are influenced by the Al content. The CO_2 peak in the high temperature range 700-800 °C can be assigned to the reduction of bulk Al-Ce oxide [14].

Fig. 4(B) shows the H_2 formation during CO-TPR. The appearance of H_2, with a peak centered at approximately 300 °C, is attributed to the water-gas shift reaction of surface hydroxyl groups remaining on the Al-Ce oxides even after the pretreatment. The addition of Al to ceria gradually improves the H_2 production. The H_2 production is in the order Pt/0.20Al-0.80Ce>Pt/0.15Al-0.85Ce>Pt/0.10Al-0.90Ce>Pt/0.05Al-0.95Ce>Pt/CeO_2.

3. CO Oxidation

The catalytic activity of the Pt/xAl-(1-x)Ce oxide was investigated as a function of Al content in CeO_2 for temperature-programmed CO oxidation in the absence and presence of water vapor (Fig. 5). It is clear that the nature of the support would have influence on the activity for CO oxidation. All the catalysts showed 100% CO conversion below 150 °C (Table 1). It can be seen that the addition of Al to ceria up to x=0.15 improves the catalytic activity compared with that of Pt/CeO_2, with complete CO oxidation reached at 120 °C, while the Pt/0.20Al-0.80Ce oxide catalyst shows a lower CO conversion. The sequence of light-off temperatures and $T_{90\%}$ values is Pt/0.10Al-0.9Ce>Pt/0.05Al-0.95Ce>Pt/0.15Al-0.85Ce>Pt/CeO_2>Pt/0.20Al-0.80Ce. Both temperatures showed a reverse-volcano type curve with respect to the Al content.

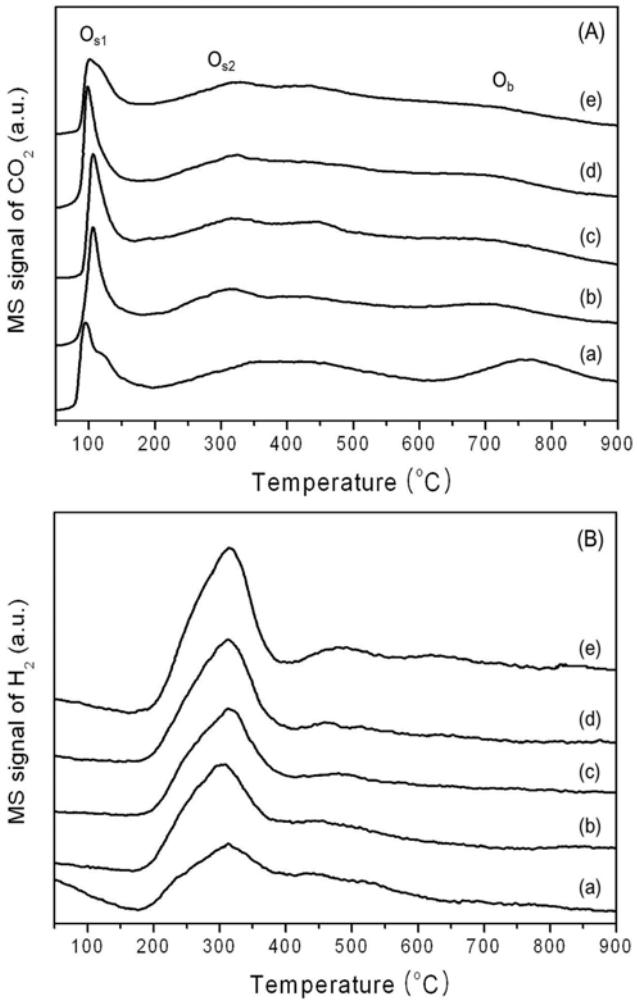

Fig. 4. CO_2 (A) and H_2 (B) production during CO-TPR over Pt/xAl-(1-x)Ce oxide catalysts: (a) Pt/CeO_2, (b) x=0.05, (c) 0.10, (d) 0.15, and (e) 0.20.

For the verification of the effect of H_2O on CO oxidation, 3% H_2O was introduced into the feed stream. The light-off curves obtained are shown in Fig. 5(B). The presence of water vapor enhances the catalytic activity and the light-off temperatures are shifted to lower temperatures ($T_{90\%}$ decreased by about 40 °C). The added water vapor acts as a reactant for the water-gas shift reaction resulting in the formation of hydrogen, which could easily reduce PtO_x to metallic Pt and in the generation of abundant hydroxyl groups which could act as better oxidants than oxygen [24-26].

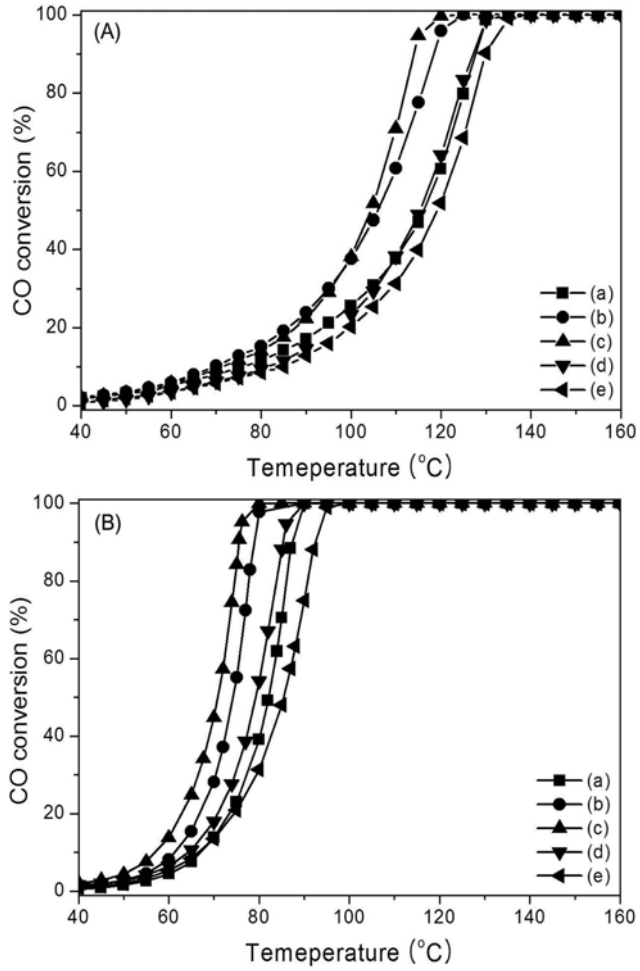

Fig. 5. CO oxidation activity as a function of reaction temperature over Pt/xAl-(1-x)Ce oxide catalysts; (a) Pt/CeO_2, (b) x=0.05, (c) 0.10, (d) 0.15, and (e) 0.20. Reaction conditions: (A) dry conditions: $CO/O_2/N_2$=1/4/95, F/W=26.8 mol h^{-1} g_{cat}^{-1}; (B) wet conditions: continuous addition of 3% H_2O.

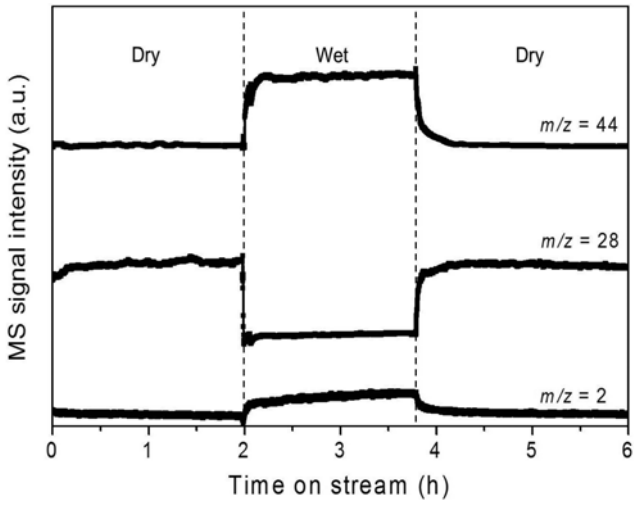

Fig. 6. Typical MS responses over the Pt/0.10Al-0.90Ce oxide catalyst during CO oxidation in dry or wet conditions; T=70 °C, Dry conditions: $CO/O_2/Ar$=1/4/95, and wet conditions: continuous addition of 3% H_2O (other conditions are the same as those under the in dry conditions).

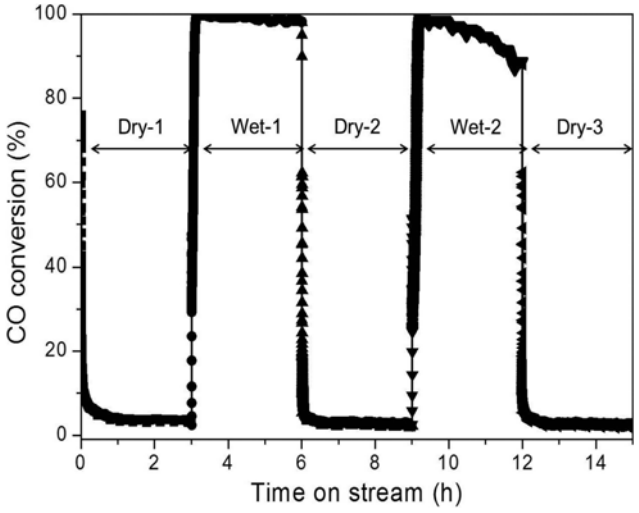

Fig. 7. Isothermal step-response experiments of CO oxidation over the Pt/0.10Al-0.90Ce oxide catalyst. Reaction conditions: T=70 °C; dry conditions: $CO/O_2/N_2$=1/4/95; wet conditions: continuous addition of 3% H_2O, and F/W=26.8 mol h^{-1} g_{cat}^{-1}.

As a probe of the reason for the increase of catalytic activity in the presence of water vapor in the feed stream, CO oxidation experiments were performed in the sequence of dry-wet-dry reaction conditions over the Pt/0.10Al-0.90Ce oxide catalyst (which showed the highest catalytic activity used in this study); the results are shown in Fig. 6. In dry conditions, low CO consumption and CO_2 formation on the Pt/0.10Al-0.90Ce oxide catalyst were observed. In wet reaction conditions, the CO concentration decreased rapidly, and CO_2 formation increased significantly as soon as the water vapor was introduced into the feed stream. In addition, the H_2 formed together with the CO_2 gradually increased with time on stream. The formation of CO_2 and H_2 can be explained by the following water-gas shift reaction: CO (s)+H_2O (g)=CO_2 (g)+H_2 (g) [27]. When the water vapor was switched off (second dry condition), the catalytic activity decreased rapidly and was restored to almost the same catalytic activity as observed in the first dry reaction. From this result, we can deduce that the enhanced catalytic activity is caused by the promotion of a water-gas shift reaction, and in particular, by the formation of H_2.

For examination of the deactivation behavior of the Pt/xAl-(1-x)Ce oxide catalyst an isothermal step-response experiment was performed at 70 °C for both sets of reaction conditions (Fig. 7). The catalytic activity on the Pt/0.10Al-0.90Ce oxide catalyst under dry conditions showed a very low conversion, which decreased continuously during the reaction. However, the CO conversion increased rapidly as soon as water vapor was introduced into the feed stream, and 100% CO conversion was showed (wet-1). The CO conversion decreased rapidly to 5% upon stopping the feed of water vapor. In the wet-2 case, the CO conversion was restored to that in the case of wet-1, but the CO conversion decreased continuously during the reaction. This phenomenon can be explained as follows: the active sites were diminished by the strongly adsorbed CO, which led to the formation of carbonate species on the catalyst surface [23]. The

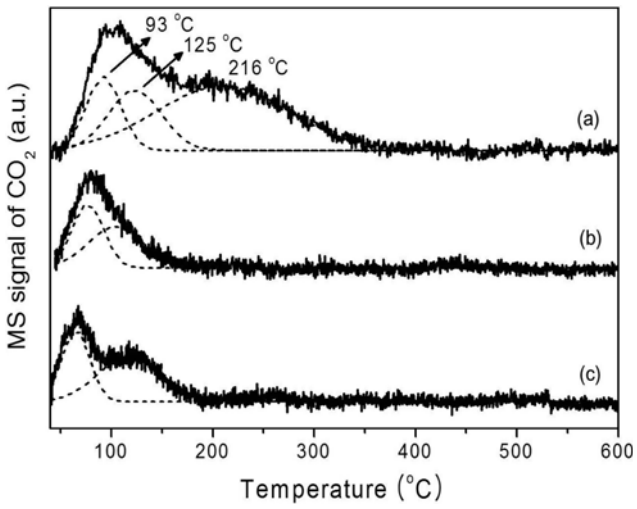

Fig. 8. CO and CO_2-TPD profiles of the Pt/0.10Al-0.90Ce oxide catalyst: CO-TPD after adsorption of (a) $CO+O_2$ (dry conditions), (b) $CO+O_2+H_2O$ (wet conditions), and (c) CO_2-TPD profile.

strongly adsorbed CO molecules under dry conditions were not completely removed at 70 °C, as evidenced by the low CO conversion under dry conditions.

Also, the catalyst can be deactivated by change in the chemical state of Pt species from Pt to PtO. Strongly adsorbed CO molecules block the active sites and finally lead to the formation of carbonates species during the reaction. Here, an attempt has been focused on the formation of carbonated-species on the catalysts surface. The CO- and CO_2-TPD profiles were measured to verify the adsorption behaviors of CO and CO_2 on the Pt/0.10Al-0.90Ce oxide catalyst during CO oxidation (Fig. 8). The desorption profiles were obtained after adsorption of the mixture $CO+O_2$ (dry) or $CO+O_2+H_2O$ (wet) on the Pt/0.10Al-0.90Ce oxide catalyst. The desorption of CO_2 is caused by the reaction between adsorbed CO and the surface or bulk oxygen of the catalyst. The CO_2 peaks were absent in the profile of the Pt-free 0.10Al-0.90Ce mixed oxide, suggesting that the CO molecules were adsorbed on the Pt species. In CO-TPD analysis, CO_2 formation was found to start immediately after the onset of the temperature increase. Broad and asymmetric peaks were observed in both TPD profiles. The TPD profiles were refined into several peaks through a deconvolution method using Gaussian function fits. Under dry conditions, three desorption peaks were observed, centered at 93, 125, and 216 °C. This means that various oxygen species were present on the 0.10Al-0.90Ce mixed oxide surface. The high-temperature peak observed under dry conditions was absent under wet conditions. This desorption peak is explained as being due to the bicarbonate species detected by IR analysis [28]. Therefore, the water vapor plays an important role in suppressing the adsorption of this species on the catalyst surface. For comparison of the desorption behaviors of the CO_2 formed by CO oxidation and the CO_2 adsorbed on the catalyst surface, CO_2-TPD was also carried out on same catalyst as shown in Fig. 8(c). Two desorption peaks of CO_2 were observed below 150 °C. The peak at 216 °C in dry conditions ($CO+O_2$) was not detected in the CO_2-TPD profiles. This means that the adsorption of CO_2 could not form the bicarbonate species, which is a factor in the deactivation for CO oxidation at an isothermal temperature of 70 °C. Therefore, we can deduce that the latter peak produced by the adsorption of CO under dry conditions, signifies the deactivation of the catalysts. Similar observations have been reported for Au/TiO_2 nanotube catalysts [28].

4. Correlation between Catalytic Activity and Catalyst Properties

It is well known that the catalytic activity is related to the metallic dispersion of the catalysts. The Pt/0.10Al-0.90Ce oxide catalyst showed the highest platinum dispersion and the lowest $T_{90\%}$ value (Table 1). In addition, the $T_{90\%}$ values shifted to higher temperatures with decreasing platinum dispersion. A linear fit can be seen between the $T_{90\%}$ values and the platinum dispersion. Therefore, the superior catalytic behavior of the Pt/0.10Al-0.90Ce oxide catalyst can be explained by its highest platinum dispersion [29,30].

The lattice oxygen is also a key factor governing CO oxidation following the Mars-van Krevelen (MvK) mechanism. A redox mechanism involving lattice oxygen/oxygen vacancy participation was proposed for CO oxidation on CeO_2 [31]. For the investigation of the correlation between the catalytic activity and the amount of CO_2 formed during CO-TPR, the correlation curve between the $T_{90\%}$ values and CO_2 formation with respect to the Al molar ratio is described in Table 1. The relative amount of CO_2 formed was calculated by integration of the mass signal of m/z=44 (CO_2) below 200 °C. The amount of CO_2 increased gradually up to an Al molar ratio of 0.10, and subsequently decreased at higher Al contents. This indicates that the Pt/0.10Al-0.90Ce oxide catalyst has the highest amount of lattice or surface oxygen, which correlates well with the trend of the $T_{90\%}$ values with respect to Al content [23].

CONCLUSIONS

Al-modified CeO_2 supports were prepared and used as supports for Pt catalysts and applied for the oxidation of CO. The surface area and pore volume increased as the Al molar ratio increased. The 1 wt% Pt/0.10Al-0.90Ce oxide catalyst showed the highest CO conversion of the catalysts investigated in dry or wet conditions. The catalytic activity in the presence of water vapor was higher than that under dry conditions. This increase in activity under wet conditions is attributed to the promotion of the water-gas shift reaction by the water vapor adsorbed on the catalyst surface. In combination with the CO chemisorption and CO-TPR experimental results, this led us to conclude that the Pt dispersion and oxygen capacity/vacancy characteristics are crucial factors in the oxidation of CO, and that the Pt/0.10Al-0.90Ce oxide catalyst has the optimal composition of those investigated in this study.

ACKNOWLEDGEMENT

This work was supported financially by a grant from the Industrial Source Technology Development Programs (2009-10033479) of the Ministry of Knowledge Economy (MKE) of Korea.

REFERENCES

1. F. Bonet, S. Grugeon, R. H. Urbina, K. Tekaia-Elhsissen and J.-M. Tarascon, *Solid State Sci.*, **4**, 665 (2002).

2. F. Mariño, C. Descorme and D. Duprez, *Appl. Catal. B: Environ.*, **58**, 175 (2005).
3. F. M. Sapountzi, M. N. Tsampas and C. G. Vayenas, *Catal. Today*, **127**, 295 (2007).
4. M. S. Chen, Y. Cai, Z. Yan, K. K. Gath, S. Axnanda and D. W. Goodman, *Surf. Sci.*, **601**, 5326 (2007).
5. S. Royer and D. Duprez, *Chem. Cat. Chem.*, **3**, 24 (2011).
6. B. Harrison, A. F. Diwell and M. Wyatt, *Platinum Metals Rev.*, **29**, 49 (1985).
7. F. Wang and G. Lu, *J. Power Sources*, **181**, 120 (2008).
8. M.-Y. Kim, J.-H. Park, C.-H. Shin, S.-W. Han and G. Seo, *Catal. Lett.*, **133**, 288 (2009).
9. Y. J. Mergler, A. van Aalst, J. van Delft and B. E. Nieuwenhuys, *Appl. Catal. B: Environ.*, **10**, 245 (1996).
10. J.-S. Bae, J.-W. Park, J.-H. Kim, J.-G. Lee, Y. Kim, and C. Han, *Korean J. Chem. Eng.*, **27**(5), 1458 (2010).
11. M.-Y. Kim, S. M. Park, J.-H. Park, C.-H. Shin, W.-J. Moon, N.-E. Sung and G. Seo, *Reac. Kinet. Mech. Cat.*, **103**, 463 (2011).
12. Y. T. Kim and E. D. Park, *Korean J. Chem. Eng.*, **27**(4), 1123 (2010).
13. G. Wu, T. Chen, X. Zong, H. J. Yan, G. Ma, X. Wang, Q. Xu, D. Wang, Z. Lei and C. Li, *J. Catal.*, **253**, 225 (2008).
14. J. Silvestre-Albero, F. Rodrýìguez-Reinoso and A. Sepúlveda-Escribano, *J. Catal.*, **210**, 127 (2002).
15. M. A Centeno, M Paulis, M Montes and J. A. Odriozola, *Appl. Catal. A: Gen*., **234**, 65 (2002).
16. S. Damyanova and J. M. C Bueno, *Appl. Catal. A: Gen.*, **253**, 135 (2003).
17. J. Papavasiliou, G. Avgouropoulos and T. Ioannides, *Appl. Catal. B: Environ.*, **69**, 226 (2007).
18. http://en.wikipedia.org/wiki/Ionic_radius.
19. J. L. Herberg, R. S. Maxwell and E. H. Majzoub, *J. Alloy. Compd.*, **417**, 39 (2006).
20. J. A. Wang, X. Bokhimi, A. Morales, O. Novaro, T. Lopez and R. Gomez, *J. Phys. Chem. B*, **103**, 299 (1999).
21. G. T. K. Fey, H. M. Kao, P. Muralidharan, T. P. Kumar and Y. D. Cho, *J. Power Sources*, **163**, 135 (2006).
22. R. Sasikala, V. Sudarsan and S. K. Kulshreshtha, *J. Solid State Chem*., **169**, 113 (2002).
23. Q. Fu, H. Saltsburg and M. Flytzani-Stephanopolutos, *Science*, **301**, 935 (2003).
24. A. Parinyaswan, S. Pongstabodee and A. Luengnaruemitchai, *Int. J. Hydrog. Energy*, **31**, 1942 (2006).
25. A. Manasilp and E. Gulari, *Appl. Catal. B: Environ.*, **37**, 17 (2002).
26. X. Yu, H. Li, S.-T. Tu, J. Yan and Z. Wang, *Int. J. Hydrog. Energy*, **36**, 3778 (2011).
27. K. G. Azzam, I. V. Babich, K. Seshan and L. Lefferts, *J. Catal.*, **251**, 153 (2007).
28. T. A. Ntho, J. A. Anderson and M. S. Scurrell, *J. Catal.*, **261**, 94 (2009).
29. C. L. Pieck, C. R. Vera, J. M. Parera, G. N. Giménez, L. R. Serra, L. S. Carvalho and M. C. Rangel, *Catal. Today*, **107-108**, 637 (2005).
30. H. Iida, K. Kondo and A. Igarashi, *Catal. Commun.*, **7**, 240 (2006).
31. W. Liu and M. Flytzani Stephanopoulos, *J. Catal.*, **153**, 304 (1995).